INTERNATIONAL JOURNAL OF RESEARCH CULTURE SOCIETY
Monthly Peer-Reviewed, Refereed, Indexed Journal
Volume - 8, Issue - 3

ISSN(O): 2456-6683
[Impact Factor: 7.148]
March - 2024

DOIs:10.2017/IJRCS/202403006 --:-- Research Paper / Article / Review

Object-Based Data Mining for Remote Sensing Image Analysis

[1]Dr. Swasti Patel, [2]Mr. Nirav Patel

[1]Assistant Professor, Department of Computer Science and Engineering, Parul University, Vadodara, India
[2] Assistant Professor, Department of Civil Engineering, Parul University, Vadodara, India

Email - [1]swastiwala16@gmail.com

Abstract: *Object-based image classification is a valuable technique for analyzing high-resolution images, particularly in delineating various landscape features based on spectral signatures like NDVI and Sfactor. In this study, six distinct classes—water bodies, forests, agriculture, scrubland, barren land, and infrastructure—are identified in a border region between Gujarat and Madhya Pradesh. A decision tree, based on NDVI and Shape factor, effectively separates these classes. Object mining, focusing on parameters like object length, area, and height, is conducted on classified objects. Correlation analysis reveals relationships among these parameters, aided by Landsat 8 imagery for multispectral data and ASTER GDEM for topographic information. Graphical representations, including scatter plots, help observe landscape characteristics.*

Key Words: *Image Processing, Object based classification, Remote Sensing, Data Mining, Landsat 8, ASTER.*

1. INTRODUCTION :

For various scientific studies, satellite imagery plays a crucial role. Data acquired from different orbiting satellites provides invaluable insights across numerous fields. This data helps predict weather patterns, understand natural disaster causes, analyze rainfall amounts, and forecast events like floods and droughts. Notably, visible satellite images resemble photographs taken from space, offering a direct visual perspective of Earth's surface.

1.1Object based image analysis

Object-based image analysis is a method utilized for analyzing digital imagery acquired from satellites. Unlike traditional pixel-based analysis, it distinguishes itself by grouping pixels with similar characteristics into single objects. This grouping is based on factors including spectral signatures, neighboring pixels, contextual information, size, and shape. Object-based classification is favored over pixel-based classification, particularly for processing Very High Resolution (VHR) imagery. This technique involves classification, segmentation, and attribution steps. GEOBIA (Geographic Object Based Image Analysis), a branch of Geographic Information System (GIS), focuses exclusively on extracting meaningful information from Remote Sensing (RS) imagery through various methods.

1.2 Scene Characterization

Scene characterization involves the intricate process of dividing the studied landscape into clearly distinct objects, utilizing a novel approach for this purpose. Information stored in the image includes both spectral and spatial data. Spatial information is derived from scene characterization, which involves identifying six classes within the stacked image. This process represents objects within the landscape and assigns them meaning. In simpler terms, a scene refers to the area on the ground surface captured by an image.

1.3 Inter relationship of objects

A land cover consists of diverse components such as water bodies, forests, deserts, rivers, irrigation fields, urban areas, towns, remote rural villages, and more. Each object within this cover is interconnected with its surroundings, offering insights into land usage patterns. This study aims to explore the relationships between objects and water bodies. Objects within a maximum distance of fifteen kilometers from water bodies are selected based on their area coverage. Those with larger areas are examined to identify interrelations.

1.4 Landsat 8 and ASTER GDM

Landsat 8, an American Earth observation satellite, is operated jointly by NASA and the USGS (United States Geological Survey) to capture images of the Earth. Its orbit moves from northeast to southwest at an inclination angle of 98.2°, situated approximately 705 kilometers above the Earth's surface. Operating across various spectra including visible, near-infrared, thermal, and shortwave infrared, it provides comprehensive data for Earth imaging. ASTER (Advanced Spaceborne Thermal and Reflection Radiometer), a Japanese satellite managed in collaboration with MITI (Ministry of International Trade and Industry) and NASA, covers nearly 99% of Earth's landmass. Its imagery is stored in GEOTIFF (Geographic Tagged Image File Format), primarily utilized for determining elevation and slope variations across different regions. Higher altitude regions typically appear white, while areas closer to sea level tend to be darker due to shadows cast by surrounding hills and mountains.

2. RELATED STUDY :

According to recent literature, object-based image analysis (OBIA) stands out as a prominent method for processing remotely sensed images, introducing a new paradigm in the field of remote sensing (Foo et al., 2017). This approach has spurred the development of dedicated software tools such as Quantum GIS, ArcGIS, ENVI, and eCognition (Bruzzone & Prieto, 2017).

The necessity for detailed information about land cover to monitor environmental changes has led to a shift from manual classification, which is time-consuming and subjective, to automated methods facilitated by OBIA (Blaschke, 2010). Rapid damage detection following natural disasters, particularly for events like landslides, relies on criteria such as slope analysis derived from remote sensing data (Van Westen et al., 2010).

Historical land cover data are crucial for understanding ecosystem dynamics, especially given the noticeable degradation caused by population growth in recent decades (Foley et al., 2005). Analyzing change detection results aids in ecosystem preservation and resource management by regulatory bodies (Cohen et al., 2016). Concerns over glacial lake melting due to global warming highlight the importance of remote sensing for early detection of potential flood events (Steiner et al., 2015).

Remote sensing, particularly using Landsat 8 imagery, has proven cost-effective for analyzing tropical cyclones and assessing damage using pre- and post-disaster images (Chen et al., 2018). Furthermore, OBIA's superiority over pixel-based methods lies in its ability to incorporate diverse information such as texture, shape, color, and spatial relationships (Baatz & Schäpe, 2000).

Image segmentation is a crucial step in OBIA, as high-quality segments serve as the foundation for subsequent analyses, providing abundant features for detailed classification (Mountrakis et al., 2011). Advanced remote sensing techniques offer more accurate classification results, including supervised and unsupervised methods tailored to the analyst's preferences (Foody, 2002).

In conclusion, OBIA, with its comprehensive approach to image analysis, offers significant advantages over traditional methods, enabling detailed environmental monitoring and disaster management. Through the integration of diverse data and advanced techniques, OBIA enhances our understanding of complex landscapes and ecosystems.

2. PROPOSED METHODOLOGY

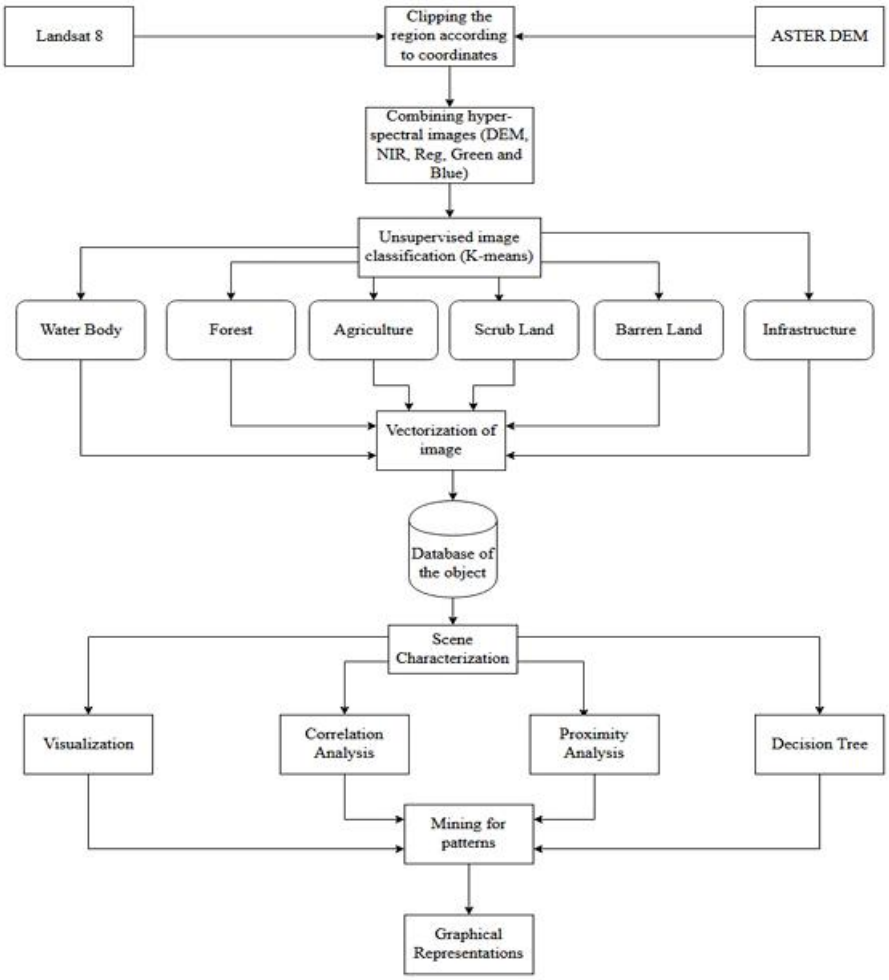

Fig 1. Flow of the proposed methodology

As demonstrated in figure 1, the proposed system is structured into two primary components. Firstly, scene characterization is conducted through decision tree analysis. Secondly, inter-relationships between classes/objects are explored by determining correlation coefficients.

The initial step involves acquiring imagery from satellites, specifically Landsat 8 and ASTER DEM. Landsat 8 provides hyperspectral images including visible, near-infrared, shortwave infrared, panchromatic, and thermal bands. ASTER DEM data are utilized for slope and elevation assessment. Due to the extensive coverage of satellite imagery, clipping is performed based on predefined latitude and longitude ranges. Once the region of interest is delineated, various layers (e.g., near-infrared, red, green, blue, and digital elevation models) are stacked together. Unsupervised classification using the k-means method is preferred in the absence of ground truth data.

2.1 Study of the Clipped Area

The region of interest (ROI) depicted in figure 2 is situated along the border of Gujarat and Madhya Pradesh. In the top-left corner lies the village of Limdi, which falls within the Jhalod Taluka in the Dohad District of Gujarat State, India. Limdi is positioned approximately 26 kilometers north of the district headquarters in Dahod. Nearby villages include Raniyar Inami, Karath, Lilva Deva, Tandi, and Raniyar Sarkari. Limdi is bordered by Limkheda Taluka to the west, Dohad Taluka to the south, Fatepura Taluka to the north, and Dahod Taluka to the south.

In the top-right corner, Panch Kheriya village is situated in the Thandla Tehsil of the Jhabua district in Madhya Pradesh, India. It is located 28 kilometers from the sub-district headquarters in Thandla and 58 kilometers from the district headquarters in Jhabua.

Moving to the bottom-left corner, Bhindol village is positioned within the Jetpur Pavi Taluka in the Vadodara District of Gujarat State, India. It is situated 91 kilometers east of the district headquarters in Vadodara, bordering the Vadodara District and Panch Mahals District. The Panch Mahal District's Jambughoda lies to the west of this village.

Lastly, in the bottom-right corner, Jhanjharwa village is located within the Ranapur Tehsil of the Jhabua district in Madhya Pradesh, India. It is situated 17 kilometers away from the sub-district headquarters in Ranapur and 37 kilometers from the district headquarters in Jhabua.

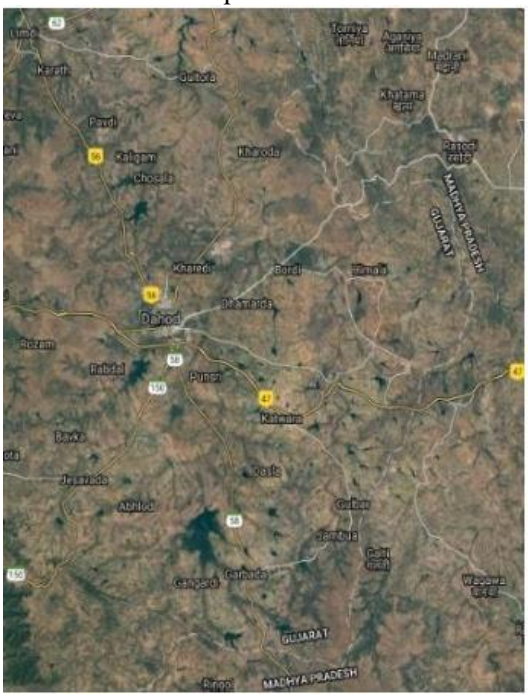

Fig 2. Study Area

The image is classified (table 4.1.1) into six main areas namely water body, forest, agriculture, scrub land, barren land and lastly infrastructure. For creating the database of the classified image, the conversion from raster format to vector format is done.

Table 1. Classes identified by performing image classification

Class Name	Examples taken as Region of Interest (ROI)	False Color Composite (FCC) Representation
Water body	Lakes, ponds, reservoirs, rivers, dams, glaciers, etc.	Black and navy blue
Forest	Dense trees and vegetation usually found near water body whose size is very large	Deep red
Agriculture	Agricultural fields that grows various crops	Pink and blood red
Scrub Land	Wild bushes and scarce trees	Bright green
Barren Land	No vegetation or construction	Yellowish green and brown
Infrastructure	City, villages, towns and concrete roads	White

Database is created of all the classes individually with parameters such as Class name, parts, eastings, northings, area, length, height, xm, ym and NDVI (Normalized Difference Vegetation Index). The detailed functions of the parameters that form the database is given in table 2.

Table 2. Functions of parameters in the database

Parameter Name	Functionality
Class name	Name of the class by which the classification is made
Parts	Number of parts that are included to form one single object
Length	Distance between two farthest points
Area	Total area of a single object
Easting	Latitude of the object
Northing	Longitude of the object
Height	Elevation form the sea level of a point
Xm	Middle point from lower left coordinate which forms x- axis
Ym	Middle point from lower left coordinate which forms y- axis
NDVI	Normalized Difference Vegetation Index is used to identify whether the target being observed contains vegetation or not. Higher values of NDVI indicate that the region contains vegetation.

2.2 Image Classification

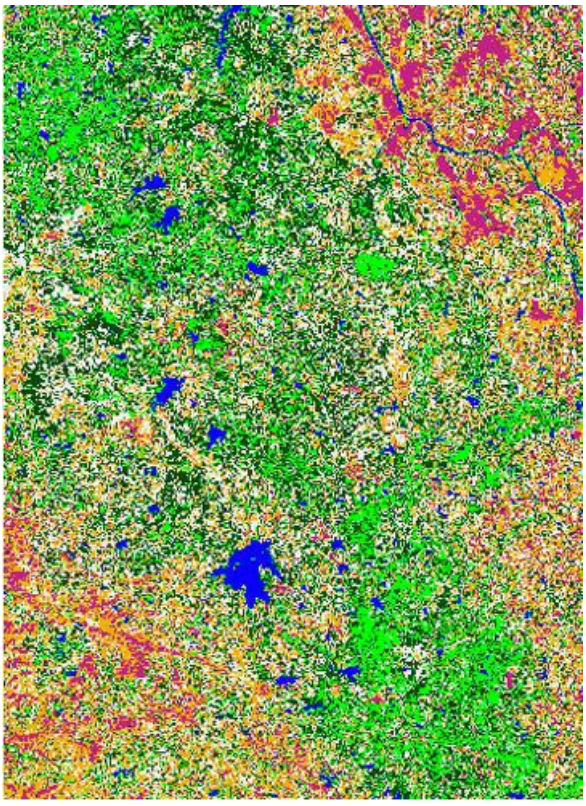

Fig 3. K-Means Classification Image

To ascertain changes in the area, it is crucial to classify the image according to its spectral attributes. Employing an unsupervised classification technique, such as the K-means algorithm, aids in this classification process. Regions of interest (ROIs) collected as training samples facilitate comparison with the ground truth of the image. The image is then classified into six distinct categories spanning its entirety: water bodies, forests, agricultural areas, scrublands, barren lands, and infrastructure.

3. RESULT AND DISCUSSION

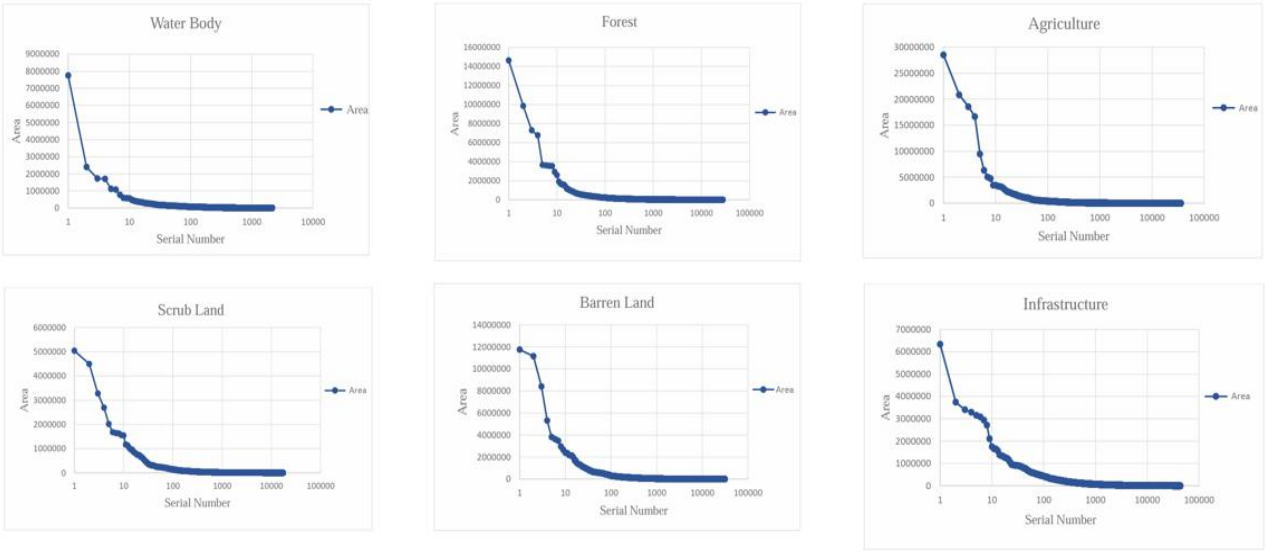

Fig 4. Graphs plotted for the entire database.

Figure 4 illustrates graphs generated from the entire database, focusing on object area analysis. These plots aid in visualizing the distribution of objects based on their area coverage, with each object mapped to its corresponding serial number. By referencing these serial numbers, one can gauge the size of the original database. For example, over two thousand objects are identified in water bodies, while forests contain approximately twenty-five thousand objects, and agricultural areas consist of over thirty thousand objects. Similarly, barren lands and infrastructure contain more than thirty-five thousand objects each. Analysis reveals that only a small proportion, roughly twenty to thirty objects across all six classes, exhibit significantly large area coverage and merit detailed scrutiny. Additionally, examination of the plotted area versus serial number graphs indicates that beyond a certain point, the area of different objects stabilizes, with the size becoming relatively insignificant in terms of area coverage.

3.1 Correlation Analysis

Six distinct classes have been identified, and for each class, a correlation matrix is computed to assess the strength and direction of the linear relationship between observed and estimated data. The Pearson correlation coefficient (r) ranges from +1 to -1, indicating perfect increasing and decreasing linear relationships, respectively. Establishing a benchmark for the correlation coefficient is essential to interpret the relationship strength effectively. For this study, a correlation coefficient greater than 0.45 denotes a moderate positive correlation, while a value below -0.45 indicates a moderate negative correlation. Values exceeding 0.75 and falling below -0.75 signify strong positive and strong negative correlations, respectively. The thresholds of 0.5 and -0.5 serve as decisive benchmarks in this analysis as shown in table 3.

$$r = \frac{n\left(\sum Y_{estimate}\, Y_{observe}\right) - \left(\sum Y_{estimate}\right)\left(\sum Y_{observe}\right)}{\sqrt{n\left(\sum Y^2_{estimate}\right) - \left(\sum Y_{estimate}\right)^2 - n\left(\sum Y^2_{observe}\right) - \left(\sum Y_{observe}\right)^2}}$$

Table 3. Correlation Matrix

Class Name	Water Body	Forest	Agriculture	Scrub Land	Barren Land	Infrastructure
Length vs Area	0.699	0.991	0.994	0.971	0.987	0.967
Length vs Height	-0.483	0.153	-0.26	-0.229	0.464	-0.168
Length vs Xm	0.275	0.053	-0.167	0.284	-0.425	0.071
Length vs Ym	0.294	-0.162	0.288	0.266	-0.476	0.018
Length vs Sfactor	-0.573	-0.556	-0.759	-0.574	-0.698	-0.574
Length vs NDVI	0.211	-0.126	-0.081	-0.157	0.161	0.329
Area vs Height	-0.154	0.19	-0.267	-0.353	0.436	-0.101
Area vs Xm	0.043	0.119	-0.185	0.375	-0.45	-0.009
Area vs Ym	0.008	-0.22	0.304	0.338	-0.424	0.121
Area vs Sfactor	-0.337	-0.521	-0.75	-0.415	-0.627	-0.589
Area vs NDVI	-0.12	-0.154	-0.083	-0.116	0.206	0.338
Height vs Xm	-0.027	0.662	0.274	-0.867	-0.658	-0.867
Height vs Ym	-0.911	-0.851	-0.8	-0.915	-0.864	-0.915
Height vs Sfactor	0.385	0.258	0.233	-0.207	-0.36	0.067
Height vs NDVI	-0.075	-0.261	0.112	-0.071	-0.085	-0.096
Xm vs Ym	-0.272	-0.853	-0.522	0.798	0.549	0.798
Xm vs Sfactor	-0.2	0.169	0.173	0.06	0.313	-0.02
Xm vs NDVI	0.204	-0.258	0.128	-0.093	0.201	-0.054
Ym vs Sfactor	-0.298	-0.003	-0.355	0.044	0.431	0.23
Ym vs NDVI	0.024	0.32	0.099	-0.017	0.153	0.13
Sfactor vs NDVI	-0.138	-0.059	-0.195	0.378	0.058	-0.074

3.2 Proximity Analysis

Vectorization provides detailed information about classified objects from the image classification process. However, considering every minute object may not yield meaningful results, as it can be both confusing and time-consuming. For mining purposes, only regions with larger surface areas were selected (see Table 4).

Table 5 displays the number of objects from each class at various distances from water bodies. Six classes were identified during the image classification process. The distance of each class is measured in kilometers relative to each water body. Analysis of Table 5 reveals that forests, agricultural fields, and infrastructure (towns, cities, villages, etc.) are predominantly found within five kilometers of water bodies. In contrast, scrublands and barren lands are less prevalent within this proximity. Both forests and agricultural fields show higher object counts up to fifteen kilometers, indicating well-planned water supply systems. The number of barren lands and scrublands is minimal within ten kilometers but increases substantially within fifteen kilometers. Infrastructure objects maintain a moderate count within ten kilometers, likely representing urban areas or towns, while those between eleven and fifteen kilometers are presumably remote villages.

3.3 Decision Tree Analysis

In Figure 5, the decision tree generated using RapidMiner Studio visually depicts the clear delineation of all classes based on NDVI and Sfactor. The tree's depth is limited to five levels, with the root node being NDVI, highlighting its significance in classifying classes hierarchically. The interpretation of the decision tree is presented in Table 6.

Classes with NDVI values less than 0.5 are identified as water bodies, as water bodies typically exhibit lower NDVI values. All other classes with NDVI values greater than 0.5 are clustered on the left side of the tree. The second level of the tree involves the shape factor, with values greater than 0.1. Scrubland and forests are categorized under this criterion, along with NDVI.

Conversely, values of the shape factor less than 0.1 encompass barren lands, infrastructure, and agriculture. Notably, the NDVI value for barren lands is not lower than that of infrastructure and agriculture. For infrastructure, a typical NDVI value is close to 0.01, while agriculture exhibits drastically lower values.

Table 4. Data scrutinization

Class/Objects	Total no. of identified objects	Total area of identified objects (sq. km.)	No. of objects chosen for mining	Total area of the chosen objects for mining (sq. km.)
Water Body	2154	449	24	226
Forest	27749	2633	24	750
Agriculture	35578	4728	23	1486
Scrub Land	17378	1380	29	400
Barren Land	30977	3354	28	829
Infrastructure	43144	4400	24	506
Total	**156980**	**16946**	**152**	**4197**

Table 5. Number of the objects of all other classes' distance from water body

Distance (in kms)	Forest	Agriculture	Scrub Land	Barren Land	Infrastructure
0 to 5	14	17	5	10	15
5 to 10	22	23	13	17	16
10 to 15	23	24	22	20	23
Total	59	64	40	47	54

Table 6. - Decision tree interpretation

Class Name	NDVI	Sfactor	NDVI	Sfactor
Water Body	≤0.5	-	-	-
Forest	>0.5	>0.102	≤0.316	-
Agriculture	>0.5	≤0.102	≤0.336	≤0.017
Scrub Land	>0.5	>0.102	>0.316	-
Barren Land	>0.5	≤0.102	>0.336	-
Infrastructure	>0.5	≤0.102	≤0.336	>0.017

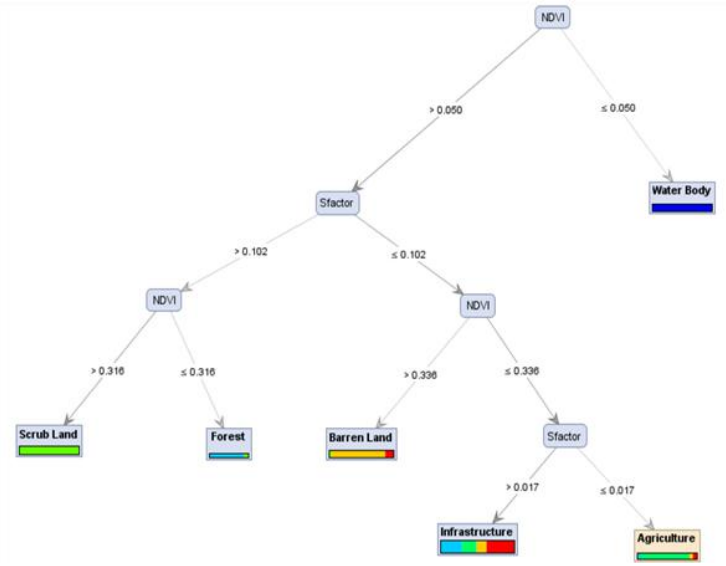

Fig 5. Decision Tree

4. CONCLUSION :

The Landsat 8 satellite, the latest in the Landsat series, orbits the Earth at an inclination angle of 98.2°, traversing from northeast to southwest. Its images are typically stored in GeoTIFF (Geographical Tagged Image File Format). Processing tools such as QGIS, ArcGIS, and ENVI were employed to merge hyper-spectral images into a multi-spectral format for analysis. The study area encompasses villages along the Gujarat-Madhya Pradesh border, spanning 1300 sq. km.

Multi-spectral images derived from Landsat data include true color and false color representations. True color images, composed of red, green, and blue (RGB) bands, provide a realistic view of the region. Conversely, false color

images integrate infrared rays, beneficial for vegetation health assessment due to their reflection by plants. ASTER provides Digital Elevation Models (DEMs) utilized for slope and elevation analysis in the region.

Region extraction based on latitude and longitude values proved time-consuming. Unsupervised k-means classification generated six classes based on distinct spectral signatures. Conversion of raster to vector formats facilitated shapefile creation, forming the basis for a comprehensive database with various parameters. Correlation coefficient calculations utilized these parameters, with resulting graphs highlighting strong correlations between length and area across all classes.

Furthermore, consistent correlations between height and slope (Ym) were observed, while shape factor (Sfactor) demonstrated a direct dependence on object length across all classes except scrub land. Notably, the length-to-height ratio for most classes did not exceed 200,000 meters, and Sfactor values remained below 6.5 for agriculture, scrub land, barren land, and infrastructure classes.

Scene characterization employed decision trees, effectively distinguishing the six classes based on Sfactor and NDVI. Future research aims to explore alternative mining techniques to uncover additional patterns among parameters.

REFERENCES :

1. Baatz, M., & Schäpe, A. (2000). Multiresolution segmentation: An optimization approach for high quality multi-scale image segmentation. Angewandte Geographische Informationsverarbeitung XII, 12(1), 12-23.
2. Blaschke, T. (2010). Object based image analysis for remote sensing. ISPRS Journal of Photogrammetry and Remote Sensing, 65(1), 2-16.
3. Bruzzone, L., & Prieto, D. F. (2017). An advanced unsupervised method to tune the parameters of object-based image analysis algorithms. IEEE Transactions on Geoscience and Remote Sensing, 55(4), 1875-1885.
4. Chen, X., Hu, X., & Ma, Y. (2018). Urban land-use change detection from multi-temporal remote sensing images using an object-based support vector machine algorithm. Remote Sensing, 10(3), 437.
5. Cohen, W. B., Yang, Z., & Kennedy, R. E. (2016). Detecting trends in forest disturbance and recovery using yearly Landsat time series: 1. LandTrendr—Temporal segmentation algorithms. Remote Sensing of Environment, 114(1), 2897-2910.
6. Foley, J. A., DeFries, R., Asner, G. P., Barford, C., Bonan, G., Carpenter, S. R., ... & Snyder, P. K. (2005). Global consequences of land use. Science, 309(5734), 570-574.
7. Foo, S., Singh, M., Tan, K. C., & Phua, M. (2017). Object-based image analysis for object identification and classification: Remote sensing technology. Springer.
8. Mountrakis, G., Im, J., & Ogole, C. (2011). Support vector machines in remote sensing: A review. ISPRS Journal of Photogrammetry and Remote Sensing, 66(3), 247-259.
9. Steiner, J. F., Pellicciotti, F., Buri, P., Miles, E. S., & Immerzeel, W. W. (2015). Modelling ice-cliff backwasting on a debris-covered glacier in the Nepalese Himalaya. Journal of Glaciology, 61(229), 889-907.
10. Van Westen, C. J., Castellanos, E., & Kuriakose, S. L. (2010). Spatial data for landslide susceptibility, hazard, and vulnerability assessment: An overview. Engineering Geology, 102(3-4), 112-131.